

Ambient Diffusion Posterior Sampling: Solving Inverse Problems with Diffusion Models trained on Corrupted Data

Asad Aali* UT Austin asad.aali@utexas.edu	Giannis Daras* UT Austin giannisdaras@utexas.edu	Brett Levac UT Austin blevac@utexas.edu
Sidharth Kumar UT Austin sidharth@utexas.edu	Alexandros G. Dimakis UT Austin dimakis@austin.utexas.edu	Jonathan I. Tamir UT Austin jtamir@utexas.edu

Abstract

We provide a framework for solving inverse problems with diffusion models learned from linearly corrupted data. Our method, *Ambient Diffusion Posterior Sampling* (A-DPS), leverages a generative model pre-trained on one type of corruption (e.g. image inpainting) to perform posterior sampling conditioned on measurements from a potentially different forward process (e.g. image blurring). We test the efficacy of our approach on standard natural image datasets (CelebA, FFHQ, and AFHQ) and we show that A-DPS can sometimes outperform models trained on clean data for several image restoration tasks in both speed and performance. We further extend the Ambient Diffusion framework to train MRI models with access only to Fourier subsampled multi-coil MRI measurements at various acceleration factors ($R=2, 4, 6, 8$). We again observe that models trained on highly subsampled data are better priors for solving inverse problems in the high acceleration regime than models trained on fully sampled data. We open-source our code and the trained Ambient Diffusion MRI models: github.com/utcsilab/ambient-diffusion-mri.

1 Introduction

For some applications, it is expensive or impossible to acquire fully observed or uncorrupted data [15, 20, 47] but possible to acquire partially observed samples. Further, in some cases, it may be desirable to train generative models with noisy or corrupted data since that reduces memorization of the training set [17, 8, 37]. Prior works have shown how to train Generative Adversarial Networks (GANs) [7, 14], flow models [29] and restoration models [32, 31, 47, 35] with corrupted training data. More recently, there has been a shift towards training *diffusion generative models* given corrupted data [17, 1, 28, 16, 30]. What remains unexplored is how to use generative models trained on a certain type of corruption (e.g. inpainted data) to solve inverse problems that arise from a different forward process (e.g. blurring). Thus far, it is not known whether models trained on corrupted data are useful priors for solving inverse problems.

We propose the first framework to solve inverse problems with diffusion models learned from linearly corrupted data, for example as in Ambient Diffusion [17]. Ambient Diffusion models estimate the *ambient score*, i.e. how to best reconstruct given an input with a corrupted linear forward operator *corrupted noisy input*. We show how to use these models for solving linear inverse problems outside of their training distribution. Our experiments on standard datasets of natural images and multi-coil

*Asad Aali and Giannis Daras contributed equally to this work.

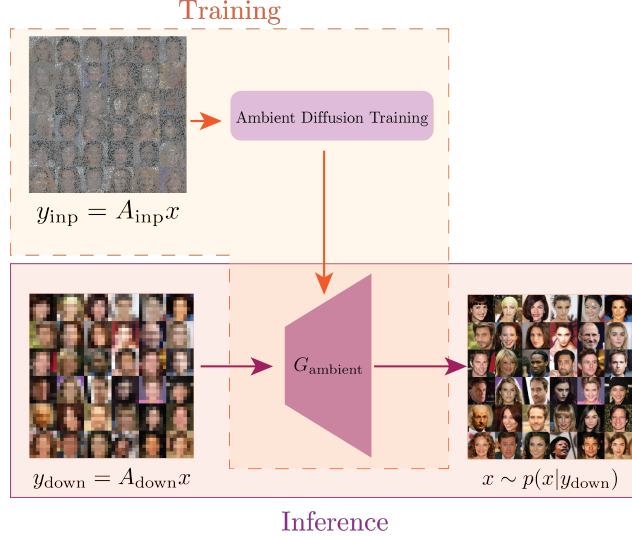


Figure 1: Illustration of Ambient Diffusion Posterior Sampling (Ambient DPS). During training, we only have access to linearly corrupted data from a forward operator A_{train} . We use this data and the Ambient Diffusion framework to learn a generative model, G_{ambient} , for the uncorrupted distribution, $p(x_0)$. At inference time, we use the learned generator to sample from the posterior distribution $p(x_0|y_{A_{\text{inf}}})$, for measurements y_{inf} coming from a different forward operator, A_{inf} .

MRI show something surprising: Ambient Models can outperform (in the high corruption regime) models trained on clean data. Further, they do so while being substantially faster. Our algorithm extends Diffusion Posterior Sampling [12] to Ambient Models and fully unlocks the potential of generative models trained on corrupted data for image restoration.

Our contributions:

1. We propose *Ambient Diffusion Posterior Sampling* (Ambient DPS), an algorithm that uses diffusion models trained on linearly corrupted data as priors for solving inverse problems with arbitrary linear measurement models.
2. We use pre-trained Ambient Diffusion models to solve inverse problems (compressed sensing, super-resolution) on several natural image datasets (CelebA, FFHQ, AFHQ) and show that they can even outperform models trained on clean data in the high corruption regime.
3. We extend the Ambient Diffusion framework to train models directly on multi-coil Fourier subsampled MRI.
4. We train Ambient Diffusion MRI models on FastMRI at various retrospective acceleration factors ($R=2, 4, 6, 8$); we again observe that models trained on subsampled data are better priors for solving inverse problems in the high acceleration regime.
5. We open-source our code and models to accelerate research in this area: github.com/utcsilab/ambient-diffusion-mri.

2 Method

2.1 Background and Notation

Diffusion Posterior Sampling (DPS). Diffusion models are typically trained (up to network reparametrizations) to reconstruct a clean image $x_0 \sim p_0(x_0)$ from a noisy observation $x_t = x_0 + \sigma_t \eta$, $\eta \sim \mathcal{N}(0, I)$. Despite the simplicity of the training objective, diffusion models can approximately sample from $p(x)$ by running a discretized version of the Stochastic Differential Equation [39, 3]:

$$dx = -2\sigma_t(\mathbb{E}[x_0|x_t] - x_t)dt + g(t)dw, \quad (2.1)$$

where \mathbf{w} is the standard Wiener process and $\mathbb{E}[\mathbf{x}_0|\mathbf{x}_t]$ is estimated by the trained neural network. Given a measurement $\mathbf{y}_{\text{inf}} = A_{\text{inf}}\mathbf{x}_0$, one can sample from the posterior distribution $p(\mathbf{x}_0|\mathbf{y}_{\text{inf}})$ by running the process:

$$d\mathbf{x} = -2\dot{\sigma}_t\sigma_t \left(\frac{\mathbb{E}[\mathbf{x}_0|\mathbf{x}_t] - \mathbf{x}_t}{\sigma_t} + \underbrace{\nabla \log p(\mathbf{y}_{\text{inf}}|\mathbf{x}_t)}_{\text{likelihood term}} \right) dt + g(t)d\mathbf{w}. \quad (2.2)$$

For most forward operators it is intractable to write the likelihood in closed form. Hence, several approximations have been proposed to use diffusion models for inverse problems [12, 27, 25, 38, 13, 19, 21]. One of the simplest and most effective approximations is Diffusion Posterior Sampling (DPS) [12]. DPS estimates \mathbf{x}_0 using \mathbf{x}_t and uses the conditional likelihood $p(\mathbf{y}_{\text{inf}}|\hat{\mathbf{x}}_0)$ instead of the intractable term, i.e. DPS approximates $p(\mathbf{y}_{\text{inf}}|\mathbf{x}_t)$ with $p(\mathbf{y}_{\text{inf}}|\mathbf{x}_0 = \mathbb{E}[\mathbf{x}_0|\mathbf{x}_t])$. The update rule becomes:

$$d\mathbf{x} = -2\dot{\sigma}_t\sigma_t \left(\frac{\mathbb{E}[\mathbf{x}_0|\mathbf{x}_t] - \mathbf{x}_t}{\sigma_t} + \gamma_t \nabla_{\mathbf{x}_t} \log p(\mathbf{y}_{\text{inf}}|\mathbf{x}_0 = \mathbb{E}[\mathbf{x}_0|\mathbf{x}_t]) \right) dt + g(t)d\mathbf{w}, \quad (2.3)$$

where γ_t is a tunable guidance parameter.

Ambient Diffusion. In some settings we do not have a large training set of clean data but we have access to a large set of lossy measurements that we would like to leverage to train a diffusion model for the clean distribution.

Daras et al. [17] considered the setting of having access to linearly corrupted data $\{\mathbf{y}_0 = A_{\text{train}}\mathbf{x}_0, A_{\text{train}}\}$, where the distribution of A_{train} , denoted as $p(A_{\text{train}})$, is assumed to be known. The ultimate goal is to learn the best restoration model given a linearly corrupted noisy input $\mathbf{y}_{t,\text{train}} = A_{\text{train}}(\mathbf{x}_0 + \sigma_t\boldsymbol{\eta})$, at all noise levels t . Daras et al. [17] form further corrupted iterates $\tilde{\mathbf{y}}_{t,\text{train}} = \tilde{A}_{\text{train}}(\mathbf{x}_0 + \sigma_t\boldsymbol{\eta})$ and train with the following objective:

$$J(\theta) = \mathbb{E}_{\mathbf{x}_0, \mathbf{x}_t, A_{\text{train}}, \tilde{A}_{\text{train}}} \left[\left\| A_{\text{train}} \mathbf{h}_\theta(\tilde{\mathbf{y}}_{0,\text{train}}, \tilde{A}_{\text{train}}) - \mathbf{y}_{t,\text{train}} \right\|^2 \right], \quad (2.4)$$

that provably learns $\mathbb{E}[\mathbf{x}_0|\tilde{A}_{\text{train}}, \tilde{\mathbf{y}}_{t,\text{train}}]$ as long as the matrix $\mathbb{E}[A_{\text{train}}^T A_{\text{train}}|\tilde{A}_{\text{train}}]$ is full-rank. In certain cases, it is possible to introduce *minimal* additional corruption and satisfy this condition. For example, if A_{train} is a random inpainting matrix (i.e. $A_{ij} \sim \text{Be}(1-p)$), then \tilde{A}_{train} can be formed by taking A_{train} and erasing additional pixels with any non-zero probability $\delta > 0$.

Multi-coil Magnetic Resonance Imaging. MRI is a prototypical use case for a framework that can learn generative models from linearly corrupted data, as in many cases it is not feasible to collect a large training set of fully sampled data [43, 18, 42]. In settings such as 3D+time dynamic contrast-enhanced MRI [49] it is impossible to collect fully sampled data due to the time-varying dynamics of the contrast agent [50].

In the multi-coil MRI setting, the acquisition involves collecting measurements of an image directly in the spatial frequency, known as k -space, from a set of spatially localized coils. Mathematically, there are N_c coils, each of which gives measurements:

$$\mathbf{z}_{\mathbf{x},i} = P\mathcal{F}S_i\mathbf{x} + \mathbf{w}_i, \quad i \in [N_c], \quad (2.5)$$

where \mathbf{x} is the (complex-valued) image of interest, S_i represents the coil-sensitivity profile of the i^{th} coil, \mathcal{F} is the (2-D or 3-D) Fourier transform, P represents the Fourier subsampling operator and \mathbf{w}_i is complex-valued Gaussian i.i.d noise. For simplicity in this work, we assume that we work in the noiseless case and we point the reader to the works of Aali et al. [1] and Kawar et al. [28] for approaches that handle the noisy case.

For the discrete approximation of the continuous signal as an image $\mathbf{x} \in C^m$, the composition of P, \mathcal{F}, S_i can be written as a matrix $A_i \in C^{m \times n}$, where the number of measurements, m , depends on the subsampling operator P . It is common to denote with R the ratio $\frac{n}{m}$, which is known as the acceleration factor. At inference time (i.e., for a new patient), we typically want to acquire data with a high acceleration factor because this reduces scan time and patient discomfort.

Due to the time required to collect k -space measurements, it is often not possible to acquire fully sampled k -space for an entire dataset. This means that training cannot rely on a fully sampled image

to guide reconstruction quality as is done in the fully supervised setting [2, 22]. To overcome this limitation, some end-to-end techniques use a loss on the measurement domain by partitioning the training measurements for each sample into (1) measurements for reconstruction, and (2) measurements for applying the loss function [47]. Other approaches leverage structure in the MRI acquisition to learn from limited-resolution data [46]. More recently, works have begun leveraging signal set properties such as group invariance to assist in learning from subsampled measurements for a variety of inverse problems [40, 36, 9, 41].

All these approaches learn a restoration model without access to fully sampled reference data. However, as they are inherently end-to-end methods, their performance on out-of-distribution tasks (e.g., due to different acquisition trajectories) is known to degrade [25, 48].

2.2 Ambient Diffusion for MRI

As explained above, the MRI acquisition process results in linearly corrupted measurements and thus it should be possible to use the Ambient Diffusion framework to learn diffusion models from the corrupted observations. Yet, we identified three important changes that differ from the setting studied by Daras et al. [17]: i) the inpainting happens in the Fourier Domain, ii) the inpainting has structure, i.e. whole vertical lines in the spatial Fourier are either observed or not observed (instead of masking random pixels) and, iii) the image is measured from an array of spatially varying receive coils. In what follows, we show how to account for these factors and apply the Ambient Diffusion framework to MRI data.

First, as in Ambient Diffusion, we will corrupt further the given measurements, but in our case, the additional corruption will happen in the Fourier space. We create further corrupted measurements for each coil by decreasing the Fourier subsampling ratio, i.e. we create iterates:

$$\tilde{z}_{\mathbf{x},i} = \tilde{P}\mathcal{F}S_i\mathbf{x}. \quad (2.6)$$

Note that this is always possible to do since we can just subsample the available data $z_{\mathbf{x},i}$. We also underline that to further corrupt the given measurements we keep the inpainting structure that there is in the measurements, i.e. we delete (at random) 2-D lines in the Fourier space (instead of independent pixel masking as in Daras et al. [17]).

In that regards the multiplicity of the coils, we combine their measurements to form a crude estimator of \mathbf{x} by taking the adjoint of \tilde{A}_{train} :

$$\tilde{\mathbf{y}}_{\text{train}} = \sum_i S_i^H \mathcal{F}^{-1}(\tilde{z}_{\mathbf{x},i}). \quad (2.7)$$

Notice that for a discrete signal $\mathbf{x} \in \mathbb{C}^n$, all these operations are linear and hence $\tilde{\mathbf{y}}$ can be written as:

$$\tilde{\mathbf{y}}_{\text{train}} = \underbrace{\left(\sum_i S_i^H \mathcal{F}^{-1} \tilde{P}\mathcal{F}S_i \right)}_{\tilde{A}_{\text{train}}} \mathbf{x}. \quad (2.8)$$

As in Ambient Diffusion, we will train the network to predict the corresponding signal before the additional corruption, i.e. our target will be:

$$\mathbf{y}_{\text{train}} = \underbrace{\left(\sum_i S_i^H \mathcal{F}^{-1} P\mathcal{F}S_i \right)}_{A_{\text{train}}} \mathbf{x}. \quad (2.9)$$

We are now ready to state our main Theorem.

Theorem 2.1 ((Informal)). *Let $\mathbf{x}_t, \mathbf{y}_{t,\text{train}}, \tilde{\mathbf{y}}_{t,\text{train}}$ represent the noisy versions of $\mathbf{x}, \mathbf{y}_{\text{train}}, \tilde{\mathbf{y}}_{\text{train}}$ respectively, i.e.:*

$$\begin{cases} \mathbf{x}_t = \mathbf{x} + \sigma_t \boldsymbol{\eta} \\ \mathbf{y}_{t,\text{train}} = A_{\text{train}} (\mathbf{y}_{t,\text{train}} + \sigma_t \boldsymbol{\eta}) \\ \tilde{\mathbf{y}}_{t,\text{train}} = \tilde{A}_{\text{train}} (\tilde{\mathbf{y}}_{t,\text{train}} + \sigma_t \boldsymbol{\eta}) \end{cases} . \quad (2.10)$$

Then, the minimizer of the objective:

$$J(\theta) = \mathbb{E}_{\mathbf{y}_{0,\text{train}}, \tilde{\mathbf{y}}_{t,\text{train}}, A_{\text{train}}, \tilde{P}} \left[\left\| A_{\text{train}} \mathbf{h}_\theta(\tilde{\mathbf{y}}_{t,\text{train}}, \tilde{P}) - \mathbf{y}_{0,\text{train}} \right\|^2 \right], \quad (2.11)$$

is: $\mathbf{h}_\theta(\tilde{\mathbf{y}}_{t,\text{train}}, \tilde{P}) = \mathbb{E}[\mathbf{x}_0 | \tilde{\mathbf{y}}_{t,\text{train}}, \tilde{P}]$.

Proof overview. The formal proof of this Theorem is given in the Appendix. We provide a sketch of the proof here. The techniques are based on Theorem 4.2 of Ambient Diffusion [17]. In Theorem 4.2, the condition that needs to be satisfied is that $\mathbb{E}[A_{\text{train}}^T A_{\text{train}} | \tilde{A}_{\text{train}}]$ is full-rank. Our objective is slightly different because the network doesn't see the whole forward operator \tilde{A}_{train} , but only part of it, i.e. the matrix \tilde{P} . By following the steps of the Ambient Diffusion proof, we arrive at the necessary condition for our case, which is to prove that $\mathbb{E}[A_{\text{train}} | \tilde{P}]$ is full-rank.

We start the argument by noting that $\mathbb{E}[P | \tilde{P}]$ is full-rank. Intuitively, this is because there is a non-zero probability of observing any Fourier coefficient and hence any deleted Fourier co-efficient could be due to the extra corruption introduced by \tilde{P} . Since \mathcal{F} is an invertible matrix, then also $\mathbb{E}[\mathcal{F}^{-1} P \mathcal{F} | \tilde{P}]$ is full-rank. Finally, we use the properties of the sensitivity masks to show that $\mathbb{E} \left[\sum_i S_i^H \mathcal{F}^{-1} P \mathcal{F} S_i | \tilde{P} \right]$ is also full-rank and this completes the proof.

Note on alternative Ambient Diffusion designs. Our approach to extending Ambient Diffusion to the Fourier subsampled MRI case is by no means unique. For example, we could have used other linear operators to aggregate the measurements from the different coils (e.g. we could have used the pseudoinverse), we could further condition on the sensitivity maps, or we could have directly fed all the coil measurements as input to the network without aggregating them. Such approaches could potentially lead to improved performance since they fully leverage the coil information. In this work, we opted for a simple and fast method (aggregation through the adjoint) and we leave such investigations for future work.

2.3 Ambient Diffusion Posterior Sampling

DPS requires access to $\mathbb{E}[\mathbf{x}_0 | \mathbf{x}_t]$ to approximately sample from $p(\mathbf{x}_0 | \mathbf{y}_{\text{inf}})$. Since Ambient Diffusion models can only work with corrupted inputs, we propose the following update rule instead:

$$d\mathbf{x} = -2\dot{\sigma}_t \sigma_t \left(\underbrace{\frac{\mathbb{E}[\mathbf{x}_0 | \mathbf{y}_{t,\text{train}}, A_{\text{train}}] - \mathbf{x}_t}{\sigma_t}}_{\text{Ambient Score}} + \gamma_t \nabla_{\mathbf{x}_t} \log p(\mathbf{y}_{\text{inf}} | \mathbf{x}_0 = \mathbb{E}[\mathbf{x}_0 | \mathbf{y}_{t,\text{train}}, A_{\text{train}}]) \right) dt + g(t) d\mathbf{w}, \quad (2.12)$$

for a fixed $A_{\text{train}} \sim p(A_{\text{train}})$. Comparing this to the DPS update rule (E.q. 2.3), all the $\mathbb{E}[\mathbf{x}_0 | \mathbf{x}_t]$ terms have been replaced with their ambient counterparts, i.e. with $\mathbb{E}[\mathbf{x}_0 | \mathbf{y}_{t,\text{train}}, A_{\text{train}}]$. We remark that similar to DPS, the proposed algorithm is an approximation to sampling from the true posterior distribution $\mathbb{E}[\mathbf{x}_0 | \mathbf{y}_{\text{inf}}]$. We term our approximate sampling algorithm for solving inverse problems with diffusion models learned from corrupted data **Ambient DPS (A-DPS)**.

2.4 Ambient Diffusion for in-domain reconstructions.

Ambient DPS can be used to solve *any* inverse problem for which the forward operator is known, using a diffusion model trained on linearly corrupted data of some form. It is important to underline though that if the inverse problem that we want to solve at inference time has the same forward operator as the one that was used for the training measurements, then we can use the Ambient Diffusion as a supervised restoration model. This is because Ambient Diffusion models are trained to estimate $\mathbb{E}[\mathbf{x}_0 | \tilde{\mathbf{y}}_{\text{train}}, \tilde{A}_{\text{train}}]$, and hence if A_{inf} comes from the same distribution as A_{train} , then, the one-step prediction of the model, Ambient One Step (A-OS), is the Mean Squared Error (MSE) minimizer. Similarly, if we are interested in unconditional generation, we can simply run Ambient DPS without the likelihood term.

3 Experiments

3.1 Ambient Diffusion with Pre-trained Models on Datasets of Natural Images

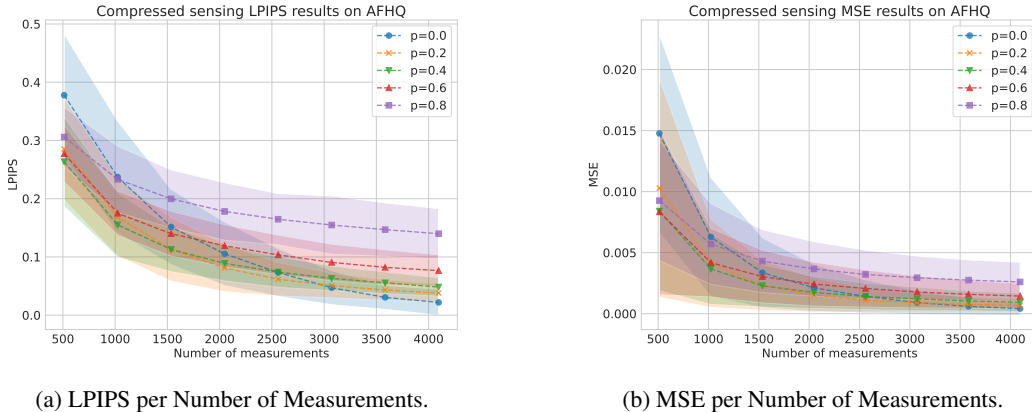


Figure 2: Compressed Sensing results, AFHQ: performance metric and standard deviation. As shown, the model trained with clean data ($p = 0.0$) only outperforms the models trained with corrupted data for more than 1000 measurements, in both LPIPS and MSE.

In this section, we evaluate the performance of Ambient DPS, which uses diffusion models trained on corrupted data, and we compare it to DPS, which uses diffusion models trained on clean data. For our experiments, we use the models from the Ambient Diffusion [17] that are trained on randomly inpainted data with different erasure probabilities. Specifically, for AFHQ we use the Ambient Models with erasure probability $p \in \{0.2, 0.4, 0.6, 0.8\}$ and for Celeb-A we use the pre-trained models with $p \in \{0.6, 0.8, 0.9\}$.

We underline that all the Ambient Models have worse performance for unconditional generation compared to the models trained with clean data (i.e. the models trained with $p = 0.0$). The goal of this work is to explore the conditional generation performance of Ambient Models, where the conditioning is in the measurements y_{inf} , and compare it with models trained on uncorrupted data. To ensure that Ambient Models do not have an unfair advantage, we test only on restoration tasks that are different from the ones encountered in their training. Specifically, we use models trained on random inpainting and we evaluate on Gaussian Compressed Sensing [4] and Super Resolution.

Hyperparameters. The only tunable parameters for DPS (Eq. 2.3) and Ambient DPS (Eq. 2.12) are in the scheduling of the magnitude of the measurements likelihood term. In all the experiments in the DPS paper, this term is kept constant throughout the diffusion sampling trajectory and the authors recommend selecting a value in the range between $[0.1, 10]$. We follow this recommendation and we keep this term constant. The value of the step size for each model is selected with a hyperparameter search in the recommended range. For all our experiments, we follow exactly the DPS implementation provided in the official code repository of the paper. The other parameter that impacts performance is the number of steps we are going to run each algorithm for, i.e. the discretization level of the SDEs of Equations 2.3, 2.12. Typically, the higher the number of steps the better the performance since the discretization error decreases [10, 11]. For the performance results, we run each method for several steps $\in \{50, 100, 150, 200, 250, 300\}$, and we report the best result among them.

Results. Figure 2 presents Gaussian Compressed Sensing reconstruction results (i.e. reconstructing a signal from Gaussian random projections). We show MSE and LPIPS performance metrics for the AFHQ dataset as we vary the number of measurements. The results are given for models that are trained with inpainted images at different levels of corruption, indicated by the erasure probability p . As shown in the Figure, the model trained with clean data outperforms the models trained with corrupted data when the number of measurements is high. However, as we reduce the number of measurements, Ambient Models outperform the models trained with clean data in the very low measurements regime. To the best of our knowledge, there is no known theoretical argument that explains this performance cross-over, and understanding this further is an interesting research

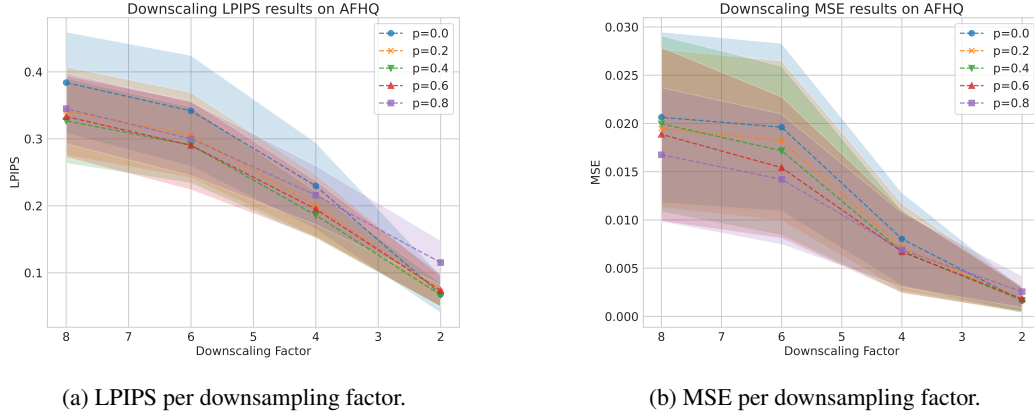


Figure 3: Super-resolution results, AFHQ: Performance metric and standard deviation. The model trained with clean data ($p = 0.0$) performs worse, except at downsampling factor 2.

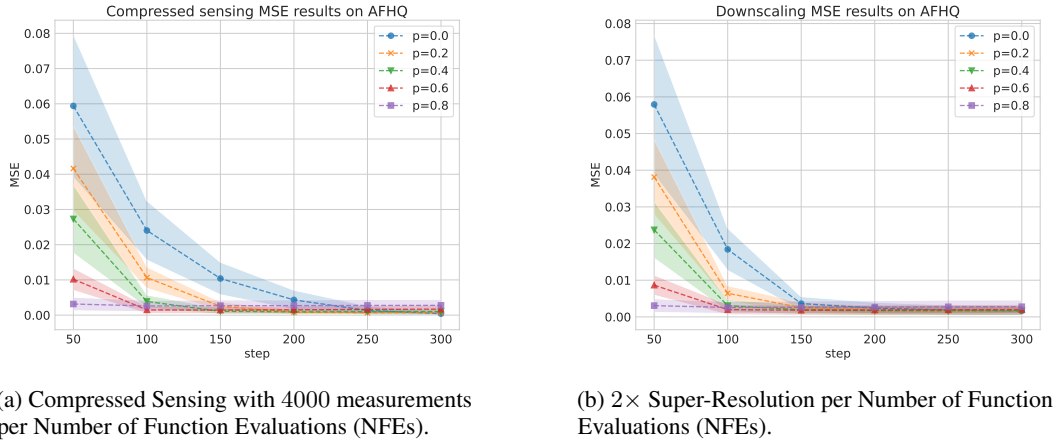


Figure 4: Speed performance plots for AFHQ.

direction. Similar results are presented in Figure 3 for the task of super-resolution at AFHQ. The model trained on clean data ($p = 0$) slightly outperforms the Ambient Models in both LPIPS and MSE for reconstructing a $2\times$ downsampled image, as expected. Yet, as the resolution decreases, there is again a cross-over in performance and models trained on corrupted data start to outperform the models trained on uncorrupted data. We include results for LPIPS and MSE for Compressed Sensing and Downsampling in FFHQ and Celeb-A in the Appendix (Figs 10, 11, 12, 13).

Finally, we examine how the number of sampling steps affects the performance. The MSE results for Compressed Sensing with 4000 measurements on AFHQ are shown in Figure 4. As shown, the higher the erasure probability p during training, the better the Compressed Sensing performance of the model for low Number of Function Evaluations (NFEs). Models trained with higher corruption are faster since they require fewer steps for the same performance. For increased NFEs, the models that are trained on clean(er) data finally outperform. This result is consistent across different datasets (AFHQ, FFHQ, CelebA), reconstruction tasks (Compressed Sensing, Downsampling), and metrics (MSE, LPIPS) (Figures 14, 15, 16, 17, 18 in the Appendix).

3.2 Ambient MRI Diffusion Models

In the previous section, we used pre-trained diffusion models on datasets of natural images. In this section, we extend Ambient Diffusion to the multi-coil Fourier subsampled MRI setting (as detailed in Section 2.2) and we train our own MRI models from scratch.

Table 1: Unconditional Sampling FID Scores for models trained on MRI data at different acceleration factors.

Inference/Training	Training Data R	Reconstruction Method	FID
EDM	1	MVUE	10.4082
EDM	2	L1-Wavelet	18.5534
EDM	4	L1-Wavelet	27.6405
EDM	6	L1-Wavelet	51.4272
EDM	8	L1-Wavelet	102.984
NCSNV2	1	MVUE	13.2006
Ambient	2	Adjoint	30.3425
Ambient	4	Adjoint	32.3101
Ambient	6	Adjoint	31.5033
Ambient	8	Adjoint	48.1525

Dataset. For the dataset preparation, we follow standard practices in the MRI literature. Specifically, we download the FastMRI dataset, randomly select 2,000 T2-Weighted scans, and pick 5 center slices from each scan. This gives us a dataset of 10,000 T2-weighted brain scans (k -space measurements). We pass each multi-channel k -space sample through a noise pre-whitening filter to transform the noise into standard white Gaussian. Then, we normalize each k -space sample by the absolute value of 99-th percentile of the root sum-of-squares reconstruction of the autocalibration region (24x24 pixels from the center). Given the pre-processed fully sampled k -space samples, we estimate sensitivity maps using the ESPIRiT calibration method [44]. These measurements serve as a fully sampled reference dataset (i.e., $R = 1$).

Sampling masks. We retrospectively subsample the k -space training data by applying randomly subsampled masks that correspond to acceleration factors $R \in \{2, 4, 6, 8\}$. The sampling masks include fully sampled vertical (readout) lines corresponding to the observed Fourier coefficients (phase encodes). We always sample the central 20 lines for autocalibration. To form further corrupted measurements, we randomly remove additional lines such that we create measurements at acceleration factor $R + 1$. For example, we take data at $R = 2$, we create further corrupted measurements at $R = 3$ and we train the model to predict the clean image by measuring its error with the available data at $R = 2$ given its prediction for the $R = 3$ corrupted input.

We note that, based on the Ambient Diffusion theory, the extra corruption is a free parameter that can be chosen to be minimal, and perhaps, we could have chosen to corrupt the available data less aggressively. Due to the lack of computational resources, we did not ablate the degree of further corruption and we leave this as future work.

Comparison Models. We train one model for each acceleration factor $R \in \{1, 2, 4, 6, 8\}$. The $R = 1$ model is trained directly on clean data (no extra corruption) based on the EDM approach [26]. The $R > 1$ models are trained with our modified Ambient Diffusion framework. While we focus on EDM for fully sampled training, we also train an NCSNV2 model for $R = 1$ following the approach in [25]. As an additional baseline, we also train models with EDM after L1-Wavelet compressed sensing reconstruction of the training set at each acceleration factor [33]. We used the BART implementation [45, 6] and searched for the best regularization parameter over the training set. Specifically, we used a regularization weighting of 0.001 with 100 iterations. We point the interested reader to Section E in the Appendix (and to our open-sourced code) for all the training hyperparameters.

Unconditional generation evaluation. We first evaluate the unconditional generation performance of each model. We show prior samples for the Ambient Diffusion models and EDM at $R = 1$ in Figure 5. Additional samples for all trained models are included in the Appendix, Figure 19. Similar

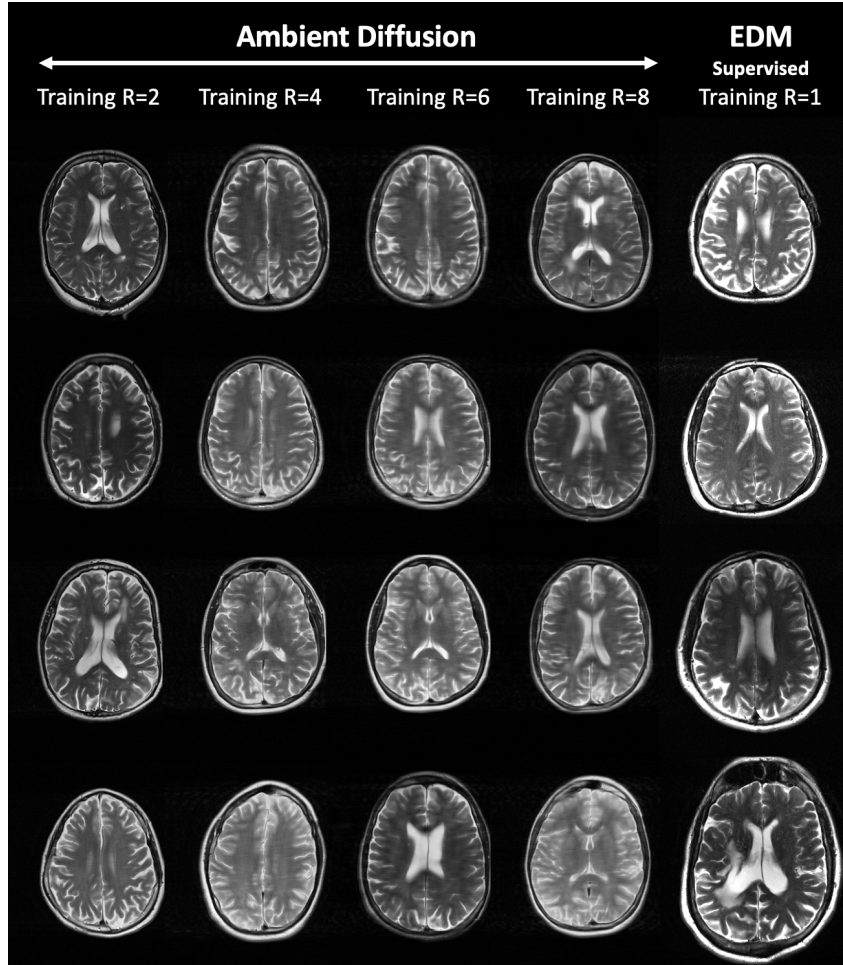


Figure 5: Prior samples from Ambient Diffusion trained with under sampled data at $R = 2, 4, 6, 8$ (columns 1 – 4), and EDM trained with fully sampled data (column 5).

to the results in Daras et al. [17], we observe that the Ambient Diffusion samples are qualitatively similar to the EDM models at low acceleration, and become slightly blurry at higher accelerations. Notably, the samples generated by Ambient Diffusion at $R = 8$ have no residual aliasing artifacts, in contrast to the samples generated from L1-Wavelet reconstructions (as seen in the Appendix).

To further quantify unconditional sample quality, we follow the approach in [5] and calculate FID scores from 100 samples using a pre-trained VGG network. Table 1, shows the FID scores for the different diffusion models. While there is an increase in FID for the Ambient models, we see that those trained at higher acceleration factors outperform the models trained on L1-Wavelet reconstructions.

3.3 MRI Reconstruction

After verifying that our trained models have learned the underlying distribution reasonably well, we want to evaluate how they perform in the task of accelerated image reconstruction. We start by listing the details of our models and the considered baselines.

Ambient Diffusion Posterior Sampling (A-DPS) We implemented our method by following Eq. 2.12 for 500 steps with a likelihood weighting $\gamma_t = \frac{1}{\|\mathbf{y} - A\mathbb{E}[\mathbf{x}_0 | \mathbf{y}_t, \text{train}, A_{\text{train}}]\|_2}$.

Ambient One Step (A-OS) As mentioned previously, our method also admits a one-step solution. This is outlined in section 2.4 by noting that we train our model to estimate $\mathbb{E}[\mathbf{x}_0 | \tilde{\mathbf{y}}_{\text{train}}, \tilde{A}_{\text{train}}]$.

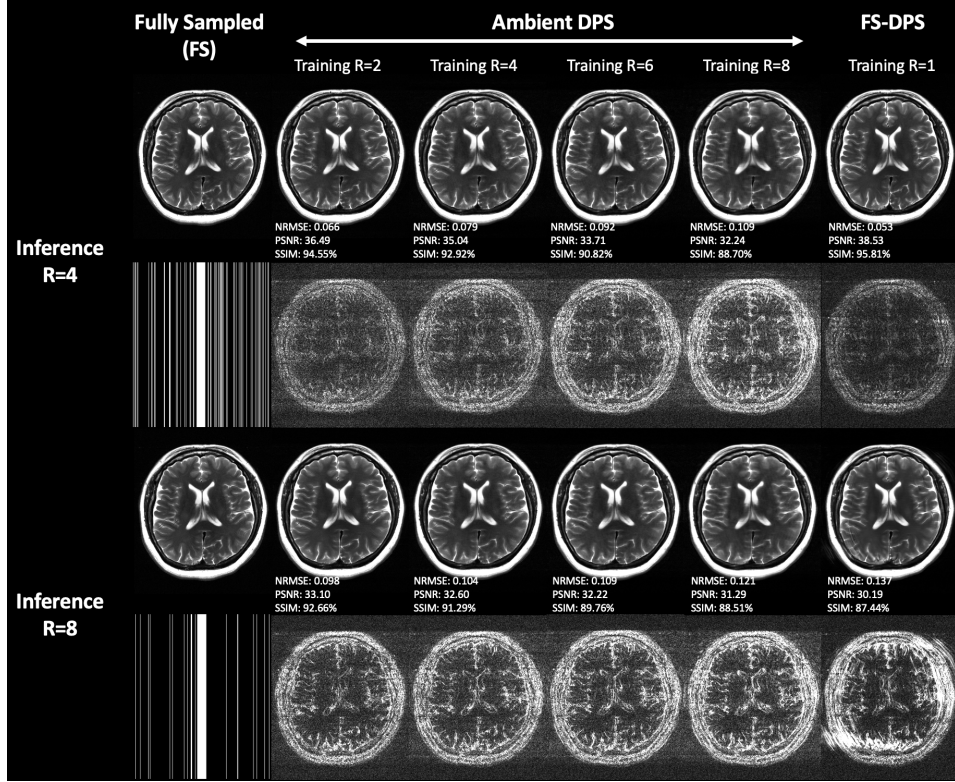


Figure 6: Posterior reconstructions using A-DPS (columns 2 – 5) and FS-DPS (column 6). Rows 1 and 3 show reconstructions at $R = 4$ and $R = 8$, respectively, while rows 2 and 4 display their difference images on a $10\times$ scale.

Thus we can use our models in a one-step fashion. The performance of the one-step prediction should only be expected to be good in-distribution, i.e. when the model is evaluated at the same acceleration factor as the one used during training.

L1-Wavelet Compressed Sensing We use the same L1-Wavelet reconstruction described previously as a standalone non-deep learning comparison.

Self-Supervised learning via Data Under-sampling (SSDU) [47] In a supervised setting, end-to-end image restoration networks can be trained by passing measurements through a network like MoDL [2] or VarNet [22] and taking a loss directly on the output of the network with the ground truth image. In the self-supervised setting, however, this is not possible. SSDU, trains the end-to-end restoration network by splitting the available measurement set (Ω) of each sample y_i^Ω into training sets (Θ) and loss sets (Λ) or measurements y_i^Θ and y_i^Λ respectively where $\Omega = \Theta \cup \Lambda$. Where the reconstruction network is given access to measurements in the training set to obtain an estimated image $\hat{x}_i^\Theta = h_\theta(y_i^\Theta)$ and the loss is then defined over the loss measurements as

$$L(y_i^\Lambda, \hat{x}_i^\Theta) = \frac{\|y_i^\Lambda - A_\Lambda \hat{x}_i^\Theta\|_1}{\|y_i^\Lambda\|_1} + \frac{\|y_i^\Lambda - A_\Lambda \hat{x}_i^\Theta\|_2}{\|y_i^\Lambda\|_2} \quad (3.1)$$

where A_Λ is the forward operator with ones in the selection mask P at only the measurement locations in the loss set and zeros elsewhere. In this work, we selected $h_\theta(\cdot)$ to have the MoDL architecture [2]. We trained individual models at four different acceleration levels ($R = 2, 4, 6, 8$). Each model was trained for ten epochs using the same training set (10,000 slices) as previously described. We used uniform random sampling to separate the training and loss measurement groups for each sample and

found that a split of $\rho = \frac{|\Lambda|}{|\Omega|} = 0.2$ provided the best performance and thus was used for reporting all subsequent metrics.

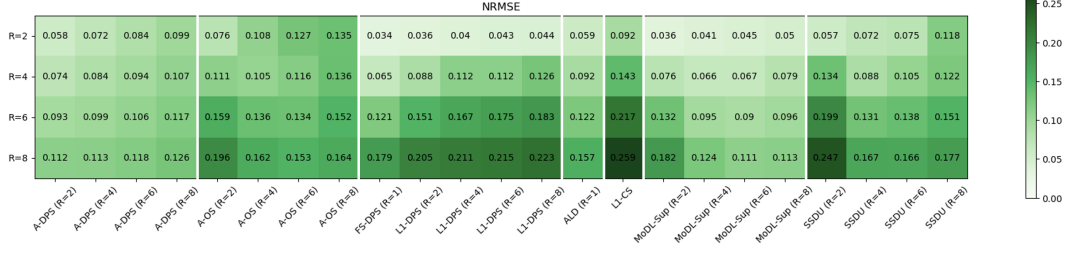


Figure 7: NRMSE performance metrics at $R = 2, 4, 6, 8$ for all methods.

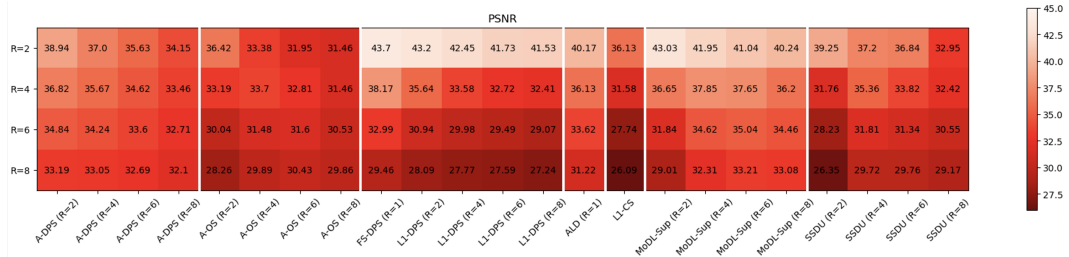


Figure 8: PSNR performance metrics at $R = 2, 4, 6, 8$ for all methods.

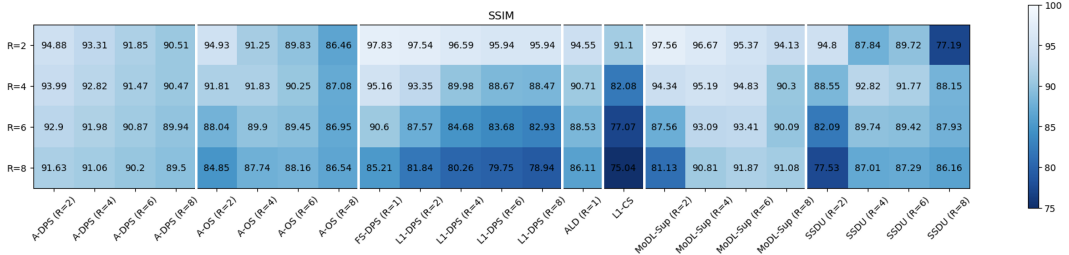


Figure 9: SSIM performance metrics at $R = 2, 4, 6, 8$ for all methods.

MoDL Supervised (MoDL-Sup) To provide an upper bound on performance for supervised end-to-end methods we also trained the MoDL architecture in a supervised fashion [2]. Again, we trained individual models at four different acceleration levels ($R = 2, 4, 6, 8$). Each model was trained using the same 10,000 slices as above. However, for these models, we used the normalized root mean squared error (NRMSE) as the loss function:

$$L(\mathbf{x}_i, \hat{\mathbf{x}}_i) = \frac{\|\mathbf{x}_i - \hat{\mathbf{x}}_i\|_2}{\|\mathbf{x}_i\|_2} \quad (3.2)$$

where \mathbf{x}_i are the ground truth images from our dataset and $\hat{\mathbf{x}}_i = \mathbf{h}_\theta(\mathbf{y}_i, A_i)$ are the reconstructions provided by our network based on under-sampled measurements \mathbf{y}_i .

Diffusion Posterior Sampling (DPS) For models trained on clean data, we can use the Diffusion Posterior Sampling (DPS) [12] algorithm. We implemented DPS with a variety of trained diffusion models. Specifically, we implemented the DPS algorithm with (1) a Diffusion model trained with fully sampled ground truth images (FS-DPS), (2 – 5) four different diffusion models trained on the LI-Wavelet reconstructions of data from measurement sets at $R = 2, 4, 6, 8$ (LI-DPS). Inference was run using the update rule of Eq. 2.3, for a total of 500 steps and with $\gamma_t = \frac{1}{\|\mathbf{y} - A\mathbb{E}[\mathbf{x}_0 | \mathbf{x}_t]\|_2}$.

Annealed Langevin Dynamics (ALD) Another popular method for solving inverse problems via score-based priors is with ALD [25]. Here we trained a score-based model using the same fully sampled 10,000 samples as above and ran inference for 1,300 steps. This method acts as another fully sampled comparison to our technique and thus serves a similar purpose as FS-DPS.

Results Quantitative metrics for the listed methods are included in Figs. 7, 8, 9 under the NRMSE, PSNR and SSIM metrics respectively. We observe that at low acceleration levels ($R = 2, 4$) FS-DPS outperforms most methods including all A-DPS models. This is not unexpected, since FS-DPS uses models trained on clean data. However, as the validation acceleration increases to higher ratios R , A-DPS begins to outperform all models, including the ones trained on fully sampled data such as FS-DPS and ALD. This trend is consistent with the results that we observed in Section 3.1 for Ambient Models trained on natural images.

To get a better sense of the performance of the different methods, we visualize reconstructions for a subset of the methods listed at various accelerations in Fig. 6. Here, we see that at lower accelerations ($R = 4$), just as the metrics suggest, FS-DPS outperforms A-DPS. However, at higher acceleration ($R = 8$) we can see that FS-DPS introduces significant artifacts into the reconstruction while our A-DPS reconstructions maintain a high degree of visual fidelity.

4 Conclusions

We presented a simple framework based on DPS for solving inverse problems with Ambient Diffusion models. We showed that diffusion models trained on missing data are state-of-the-art inverse problem solvers for high corruption levels even if the forward process at inference time is different from the one used during training. Our framework fully unlocks the potential of Ambient Diffusion models that are critical in applications where access to full data is impossible or undesirable.

5 Acknowledgements

This research has been supported by NSF Grants CCF 1763702, NSF CCF-2239687 (CAREER), AF 1901292, CNS 2148141, Tripods CCF 1934932, NSF AI Institute for Foundations of Machine Learning (IFML) 2019844, Oracle for Research Fellowship, Google Research Scholars Award, the Texas Advanced Computing Center (TACC) and research gifts by Western Digital, WNCG IAP, UT Austin Machine Learning Lab (MLL), Cisco and the Archie Straiton Endowed Faculty Fellowship. Giannis Daras has been supported by the Onassis Fellowship (Scholarship ID: F ZS 012-1/2022-2023), the Bodossaki Fellowship and the Leventis Fellowship.

References

- [1] Asad Aali, Marius Arvinte, Sidharth Kumar, and Jonathan I Tamir. “Solving Inverse Problems with Score-Based Generative Priors learned from Noisy Data”. In: *arXiv preprint arXiv:2305.01166* (2023) (pages 1, 3).
- [2] Hemant K. Aggarwal, Merry P. Mani, and Mathews Jacob. “MoDL: Model-Based Deep Learning Architecture for Inverse Problems”. In: *IEEE Transactions on Medical Imaging* 38.2 (2019), pp. 394–405. DOI: [10.1109/TMI.2018.2865356](https://doi.org/10.1109/TMI.2018.2865356) (pages 4, 10, 11).
- [3] Brian D.O. Anderson. “Reverse-time diffusion equation models”. In: *Stochastic Processes and their Applications* 12.3 (1982), pp. 313–326 (page 2).
- [4] Richard G Baraniuk. “Compressive sensing [lecture notes]”. In: *IEEE signal processing magazine* 24.4 (2007), pp. 118–121 (page 6).
- [5] Matthew Bendel, Rizwan Ahmad, and Philip Schniter. “A Regularized Conditional GAN for Posterior Sampling in Image Recovery Problems”. In: *arXiv e-prints*, arXiv:2210.13389 (Oct. 2022), arXiv:2210.13389. DOI: [10.48550/arXiv.2210.13389](https://doi.org/10.48550/arXiv.2210.13389). arXiv: [2210.13389](https://arxiv.org/abs/2210.13389) [cs.CV] (page 9).
- [6] Moritz Blumenthal, Christian Holme, Volkert Roeloffs, Sebastian Rosenzweig, Philip Schaten, Nick Scholand, Jon Tamir, Xiaoqing Wang, and Martin Uecker. *mrirecon/bart: version 0.8.00*. Version 0.8.00. Sept. 2022. DOI: [10.5281/zenodo.7110562](https://doi.org/10.5281/zenodo.7110562). URL: <https://doi.org/10.5281/zenodo.7110562> (page 8).
- [7] Ashish Bora, Eric Price, and Alexandros G Dimakis. “AmbientGAN: Generative models from lossy measurements”. In: *International conference on learning representations*. 2018 (page 1).
- [8] Nicolas Carlini, Jamie Hayes, Milad Nasr, Matthew Jagielski, Vikash Sehwal, Florian Tramèr, Borja Balle, Daphne Ippolito, and Eric Wallace. “Extracting training data from diffusion models”. In: *32nd USENIX Security Symposium (USENIX Security 23)*. 2023, pp. 5253–5270 (page 1).
- [9] Dongdong Chen, Julián Tachella, and Mike E. Davies. “Robust Equivariant Imaging: A Fully Unsupervised Framework for Learning To Image From Noisy and Partial Measurements”. In: *Proceedings of the IEEE/CVF Conference on Computer Vision and Pattern Recognition (CVPR)*. June 2022, pp. 5647–5656 (page 4).
- [10] Sitan Chen, Sinho Chewi, Jerry Li, Yuanzhi Li, Adil Salim, and Anru R Zhang. “Sampling is as easy as learning the score: theory for diffusion models with minimal data assumptions”. In: *arXiv preprint arXiv:2209.11215* (2022) (page 6).
- [11] Sitan Chen, Giannis Daras, and Alex Dimakis. “Restoration-degradation beyond linear diffusions: A non-asymptotic analysis for ddim-type samplers”. In: *International Conference on Machine Learning*. PMLR. 2023, pp. 4462–4484 (page 6).
- [12] Hyungjin Chung, Jeongsol Kim, Michael Thompson Mccann, Marc Louis Klasky, and Jong Chul Ye. “Diffusion Posterior Sampling for General Noisy Inverse Problems”. In: *The Eleventh International Conference on Learning Representations*. 2023. URL: <https://openreview.net/forum?id=0nD9zGAGT0k> (pages 2, 3, 11).
- [13] Hyungjin Chung, Byeongsu Sim, Dohoon Ryu, and Jong Chul Ye. “Improving diffusion models for inverse problems using manifold constraints”. In: *Advances in Neural Information Processing Systems* 35 (2022), pp. 25683–25696 (page 3).
- [14] Elizabeth K. Cole, Frank Ong, Shreyas S. Vasanawala, and John M. Pauly. “Fast Unsupervised MRI Reconstruction Without Fully-Sampled Ground Truth Data Using Generative Adversarial Networks”. In: *2021 IEEE/CVF International Conference on Computer Vision Workshops (ICCVW)*. 2021, pp. 3971–3980. DOI: [10.1109/ICCVW54120.2021.00444](https://doi.org/10.1109/ICCVW54120.2021.00444) (page 1).
- [15] The Event Horizon Telescope Collaboration et al. “First M87 Event Horizon Telescope Results. IV. Imaging the Central Supermassive Black Hole”. In: *The Astrophysical Journal Letters* 875.1 (Apr. 2019), p. L4. DOI: [10.3847/2041-8213/ab0e85](https://doi.org/10.3847/2041-8213/ab0e85). URL: <https://dx.doi.org/10.3847/2041-8213/ab0e85> (page 1).
- [16] Zhuo-Xu Cui, Chentao Cao, Shaonan Liu, Qingyong Zhu, Jing Cheng, Haifeng Wang, Yanjie Zhu, and Dong Liang. “Self-score: Self-supervised learning on score-based models for mri reconstruction”. In: *arXiv preprint arXiv:2209.00835* (2022) (page 1).
- [17] Giannis Daras, Kulin Shah, Yuval Dagan, Aravind Gollakota, Alexandros G Dimakis, and Adam Klivans. “Ambient Diffusion: Learning Clean Distributions from Corrupted Data”. In: *arXiv preprint arXiv:2305.19256* (2023) (pages 1, 3–6, 9, 16, 22).

- [18] Arjun D Desai, Andrew M Schmidt, Elka B Rubin, Christopher M Sandino, Marianne S Black, Valentina Mazzoli, Kathryn J Stevens, Robert Boutin, Christopher Ré, Garry E Gold, Brian A Hargreaves, and Akshay S Chaudhari. *SKM-TEA: A Dataset for Accelerated MRI Reconstruction with Dense Image Labels for Quantitative Clinical Evaluation*. 2022. arXiv: [2203.06823](https://arxiv.org/abs/2203.06823) [eess.IV] (page 3).
- [19] Berthy T Feng, Jamie Smith, Michael Rubinstein, Huiwen Chang, Katherine L Bouman, and William T Freeman. “Score-Based diffusion models as principled priors for inverse imaging”. In: *arXiv preprint arXiv:2304.11751* (2023) (page 3).
- [20] Angela F Gao, Oscar Leong, He Sun, and Katherine L Bouman. “Image Reconstruction without Explicit Priors”. In: *ICASSP 2023-2023 IEEE International Conference on Acoustics, Speech and Signal Processing (ICASSP)*. IEEE. 2023, pp. 1–5 (page 1).
- [21] Alexandros Graikos, Nikolay Malkin, Nebojsa Jojic, and Dimitris Samaras. “Diffusion models as plug-and-play priors”. In: *Advances in Neural Information Processing Systems 35* (2022), pp. 14715–14728 (page 3).
- [22] Kerstin Hammernik, Teresa Klatzer, Erich Kobler, Michael P. Recht, Daniel K. Sodickson, Thomas Pock, and Florian Knoll. “Learning a variational network for reconstruction of accelerated MRI data”. In: *Magnetic Resonance in Medicine* 79.6 (2018), pp. 3055–3071. DOI: <https://doi.org/10.1002/mrm.26977>. eprint: <https://onlinelibrary.wiley.com/doi/pdf/10.1002/mrm.26977>. URL: <https://onlinelibrary.wiley.com/doi/abs/10.1002/mrm.26977> (pages 4, 10).
- [23] Reinhard Heckel and Paul Hand. *Deep Decoder: Concise Image Representations from Untrained Non-convolutional Networks*. 2019. arXiv: [1810.03982](https://arxiv.org/abs/1810.03982) [cs.CV].
- [24] Yuyang Hu, Mauricio Delbracio, Peyman Milanfar, and Ulugbek S. Kamilov. “A Restoration Network as an Implicit Prior”. In: (2023). arXiv:2310.01391.
- [25] Ajil Jalal, Marius Arvinte, Giannis Daras, Eric Price, Alexandros G Dimakis, and Jon Tamir. “Robust compressed sensing mri with deep generative priors”. In: *Advances in Neural Information Processing Systems 34* (2021), pp. 14938–14954 (pages 3, 4, 8, 12).
- [26] Tero Karras, Miika Aittala, Timo Aila, and Samuli Laine. “Elucidating the design space of diffusion-based generative models”. In: *arXiv preprint arXiv:2206.00364* (2022) (page 8).
- [27] Bahjat Kawar, Michael Elad, Stefano Ermon, and Jiaming Song. “Denoising Diffusion Restoration Models”. In: *Advances in Neural Information Processing Systems* (page 3).
- [28] Bahjat Kawar, Noam Elata, Tomer Michaeli, and Michael Elad. “GSURE-Based Diffusion Model Training with Corrupted Data”. In: *arXiv preprint arXiv:2305.13128* (2023) (pages 1, 3).
- [29] Varun A Kelkar, Rucha Deshpande, Arindam Banerjee, and Mark A Anastasio. “Ambient-Flow: Invertible generative models from incomplete, noisy measurements”. In: *arXiv preprint arXiv:2309.04856* (2023) (page 1).
- [30] Kwanyoung Kim and Jong Chul Ye. “Noise2score: tweedie’s approach to self-supervised image denoising without clean images”. In: *Advances in Neural Information Processing Systems 34* (2021), pp. 864–874 (page 1).
- [31] Alexander Krull, Tim-Oliver Buchholz, and Florian Jug. “Noise2void-learning denoising from single noisy images”. In: *Proceedings of the IEEE/CVF conference on computer vision and pattern recognition*. 2019, pp. 2129–2137 (page 1).
- [32] Jaakko Lehtinen, Jacob Munkberg, Jon Hasselgren, Samuli Laine, Tero Karras, Miika Aittala, and Timo Aila. “Noise2Noise: Learning image restoration without clean data”. In: *arXiv preprint arXiv:1803.04189* (2018) (page 1).
- [33] Michael Lustig, David Donoho, and John M. Pauly. “Sparse MRI: The application of compressed sensing for rapid MR imaging”. In: *Magnetic Resonance in Medicine* 58.6 (2007), pp. 1182–1195. DOI: <https://doi.org/10.1002/mrm.21391>. eprint: <https://onlinelibrary.wiley.com/doi/pdf/10.1002/mrm.21391>. URL: <https://onlinelibrary.wiley.com/doi/abs/10.1002/mrm.21391> (page 8).
- [34] Christopher A Metzler, Arian Maleki, and Richard G Baraniuk. “From denoising to compressed sensing”. In: *IEEE Transactions on Information Theory* 62.9 (2016), pp. 5117–5144.
- [35] Charles Millard and Mark Chiew. “A Theoretical Framework for Self-Supervised MR Image Reconstruction Using Sub-Sampling via Variable Density Noisier2Noise”. In: *IEEE Transactions on Computational Imaging* 9 (2023), pp. 707–720. DOI: [10.1109/TCI.2023.3299212](https://doi.org/10.1109/TCI.2023.3299212) (page 1).

- [36] Jérémy Scanvic, Mike Davies, Patrice Abry, and Julián Tachella. *Self-Supervised Learning for Image Super-Resolution and Deblurring*. 2023. arXiv: [2312.11232](https://arxiv.org/abs/2312.11232) [eess.IV] (page 4).
- [37] Gowthami Somepalli, Vasu Singla, Micah Goldblum, Jonas Geiping, and Tom Goldstein. “Diffusion Art or Digital Forgery? Investigating Data Replication in Diffusion Models”. In: *arXiv preprint arXiv:2212.03860* (2022) (page 1).
- [38] Yang Song, Liyue Shen, Lei Xing, and Stefano Ermon. “Solving inverse problems in medical imaging with score-based generative models”. In: *arXiv preprint arXiv:2111.08005* (2021) (page 3).
- [39] Yang Song, Jascha Sohl-Dickstein, Diederik P Kingma, Abhishek Kumar, Stefano Ermon, and Ben Poole. “Score-based generative modeling through stochastic differential equations”. In: *arXiv preprint arXiv:2011.13456* (2020) (page 2).
- [40] Julián Tachella, Dongdong Chen, and Mike Davies. *Sensing Theorems for Unsupervised Learning in Linear Inverse Problems*. 2022. arXiv: [2203.12513](https://arxiv.org/abs/2203.12513) [stat.ML] (page 4).
- [41] Julián Tachella, Dongdong Chen, and Mike Davies. “Unsupervised Learning From Incomplete Measurements for Inverse Problems”. In: *arXiv preprint arXiv:2201.12151* (2022) (page 4).
- [42] U Tariq, P Lai, M Lustig, M Alley, M Zhang, G Gold, and Vasanaawala Shreyas S. *MRI Data: Undersampled Knees*. URL: <http://old.mridata.org/undersampled/knees> (page 3).
- [43] Radhika Tibrewala, Tarun Dutt, Angela Tong, Luke Ginocchio, Mahesh B Keerthivasan, Steven H Baete, Sumit Chopra, Yvonne W Lui, Daniel K Sodickson, Hersh Chandarana, and Patricia M Johnson. *FastMRI Prostate: A Publicly Available, Biparametric MRI Dataset to Advance Machine Learning for Prostate Cancer Imaging*. 2023. arXiv: [2304.09254](https://arxiv.org/abs/2304.09254) [physics.med-ph] (page 3).
- [44] Martin Uecker, Peng Lai, Mark J. Murphy, Patrick Virtue, Michael Elad, John M. Pauly, Shreyas S. Vasanawala, and Michael Lustig. “ESPIRiT—an eigenvalue approach to autocalibrating parallel MRI: Where SENSE meets GRAPPA”. In: *Magnetic Resonance in Medicine* 71.3 (2014), pp. 990–1001. DOI: <https://doi.org/10.1002/mrm.24751>. eprint: <https://onlinelibrary.wiley.com/doi/pdf/10.1002/mrm.24751>. URL: <https://onlinelibrary.wiley.com/doi/abs/10.1002/mrm.24751> (page 8).
- [45] Martin Uecker, Jonathan I Tamir, Frank Ong, and Michael Lustig. “The BART toolbox for computational magnetic resonance imaging”. In: *Proc Intl Soc Magn Reson Med*. Vol. 24. 2016 (page 8).
- [46] Frederic Wang, Han Qi, Alfredo De Goyeneche, Reinhard Heckel, Michael Lustig, and Efrat Shimron. “K-band: Self-supervised MRI Reconstruction via Stochastic Gradient Descent over K-space Subsets”. In: *arXiv e-prints*, arXiv:2308.02958 (Aug. 2023), arXiv:2308.02958. DOI: [10.48550/arXiv.2308.02958](https://arxiv.org/abs/2308.02958). arXiv: [2308.02958](https://arxiv.org/abs/2308.02958) [eess.IV] (page 4).
- [47] Burhaneddin Yaman, Seyed Amir Hossein Hosseini, Steen Moeller, Jutta Ellermann, Kâmil Uğurbil, and Mehmet Akçakaya. “Self-supervised learning of physics-guided reconstruction neural networks without fully sampled reference data”. In: *Magnetic Resonance in Medicine* 84.6 (2020), pp. 3172–3191. DOI: <https://doi.org/10.1002/mrm.28378>. eprint: <https://onlinelibrary.wiley.com/doi/pdf/10.1002/mrm.28378>. URL: <https://onlinelibrary.wiley.com/doi/abs/10.1002/mrm.28378> (pages 1, 4, 10).
- [48] Martin Zach, Florian Knoll, and Thomas Pock. “Stable Deep MRI Reconstruction using Generative Priors”. In: *arXiv e-prints*, arXiv:2210.13834 (Oct. 2022), arXiv:2210.13834. DOI: [10.48550/arXiv.2210.13834](https://arxiv.org/abs/2210.13834). arXiv: [2210.13834](https://arxiv.org/abs/2210.13834) [eess.IV] (page 4).
- [49] Tao Zhang, Joseph Y. Cheng, Aaron G. Potnick, Richard A. Barth, Marcus T. Alley, Martin Uecker, Michael Lustig, John M. Pauly, and Shreyas S. Vasanawala. “Fast pediatric 3D free-breathing abdominal dynamic contrast enhanced MRI with high spatiotemporal resolution”. In: *Journal of Magnetic Resonance Imaging* 41.2 (2015), pp. 460–473. DOI: <https://doi.org/10.1002/jmri.24551>. eprint: <https://onlinelibrary.wiley.com/doi/pdf/10.1002/jmri.24551>. URL: <https://onlinelibrary.wiley.com/doi/abs/10.1002/jmri.24551> (page 3).
- [50] Tao Zhang, John Pauly, Shreyas Vasanawala, and Michael Lustig. *MRI Data: Undersampled Abdomens*. URL: <http://old.mridata.org/undersampled/abdomens> (page 3).
- [51] Hongkai Zheng, Weili Nie, Arash Vahdat, and Anima Anandkumar. “Fast Training of Diffusion Models with Masked Transformers”. In: *arXiv preprint arXiv:2306.09305* (2023).

A Theorem Proof

In this section, we provide the proof of Theorem 2.1 that was stated in the main paper. We begin by giving the formal statement of the theorem.

Theorem A.1 (Formal Statement of Theorem 2.1). *Let $\mathbf{x} \in \mathbb{C}^n$ be an unknown signal from a distribution that admits density $p(\mathbf{x})$. Let $\{S_i\}$ be a random set of diagonal matrices $\in \mathbb{C}^n$ that satisfies: $\sum_i S_i^H S_i = I_{n \times n}$. Assume sample access to linearly corrupted measurements of \mathbf{x} given by:*

$$\mathbf{y}_{\text{train}} = \underbrace{\left(\sum_i S_i^H \mathcal{F}^{-1} P \mathcal{F} S_i \right)}_{A_{\text{train}}} \mathbf{x}, \quad (\text{A.1})$$

where \mathcal{F} is the discrete Fourier matrix and P is a random inpainting matrix, i.e. a diagonal matrix with either zeros or ones in the diagonal, such that $\Pr[P_{ii} = 1] > 0$, for all entries i of the diagonal. Define:

$$\tilde{\mathbf{y}}_{\text{train}} = \underbrace{\left(\sum_i S_i^H \mathcal{F}^{-1} \tilde{P} \mathcal{F} S_i \right)}_{\tilde{A}_{\text{train}}} \mathbf{x}, \quad (\text{A.2})$$

where \tilde{P} is a further corrupted version of P in the sense that with some non-zero probability p , a diagonal element that was 1 in P becomes 0 in \tilde{P} . Define also $\mathbf{x}_t, \mathbf{y}_{t,\text{train}}, \tilde{\mathbf{y}}_{t,\text{train}}$ the noisy versions of $\mathbf{x}, \mathbf{y}_{\text{train}}, \tilde{\mathbf{y}}_{\text{train}}$ respectively, as in:

$$\mathbf{x}_t = \mathbf{x} + \sigma_t \boldsymbol{\eta}, \quad \mathbf{y}_{t,\text{train}} = A_{\text{train}} (\mathbf{y}_{t,\text{train}} + \sigma_t \boldsymbol{\eta}), \quad \tilde{\mathbf{y}}_{t,\text{train}} = \tilde{A}_{\text{train}} (\tilde{\mathbf{y}}_{t,\text{train}} + \sigma_t \boldsymbol{\eta}). \quad (\text{A.3})$$

Then, the minimizer of the objective:

$$J(\theta) = \mathbb{E}_{\mathbf{y}_{0,\text{train}}, \tilde{\mathbf{y}}_{t,\text{train}}, A_{\text{train}}, \tilde{P}} \left[\left\| A_{\text{train}} \mathbf{h}_\theta(\tilde{\mathbf{y}}_{t,\text{train}}, \tilde{P}) - \mathbf{y}_{0,\text{train}} \right\|^2 \right], \quad (\text{A.4})$$

is: $\mathbf{h}_\theta(\tilde{\mathbf{y}}_{t,\text{train}}, \tilde{P}) = \mathbb{E}[\mathbf{x}_0 | \tilde{\mathbf{y}}_{t,\text{train}}, \tilde{P}]$.

Proof. We adapt the proof Theorem 4.1 in Ambient Diffusion [17]. To avoid notation clutter, we will be omitting the subscript “train”, when necessary.

Let $\mathbf{h}_{\theta^*}(\tilde{\mathbf{y}}_t, \tilde{P}) = \mathbb{E}[\mathbf{x}_0 | \tilde{\mathbf{y}}_t, \tilde{P}] + \mathbf{f}(\tilde{\mathbf{y}}_t, \tilde{P})$ be the optimal solution. The value of the objective for the optimal solution becomes:

$$\begin{aligned} J(\theta^*) &= \mathbb{E}_{\mathbf{y}_0, \tilde{\mathbf{y}}_t, A, \tilde{P}} \left[\left\| A \mathbb{E}[\mathbf{x}_0 | \tilde{\mathbf{y}}_t, \tilde{P}] + A \mathbf{f}(\tilde{\mathbf{y}}_t, \tilde{P}) - \mathbf{y}_0 \right\|^2 \right] \quad (\text{A.5}) \\ &= \mathbb{E}_{\mathbf{y}_0, \tilde{\mathbf{y}}_t, A, \tilde{P}} \left[\underbrace{\left\| A \mathbb{E}[\mathbf{x}_0 | \tilde{\mathbf{y}}_t, \tilde{P}] - \mathbf{y}_0 \right\|^2}_{\text{irreducible error}} + \mathbf{f}(\tilde{\mathbf{y}}_t, \tilde{P})^T A^T A \mathbf{f}(\tilde{\mathbf{y}}_t, \tilde{P}) - 2 \left(\mathbb{E}[\mathbf{x}_0 | \tilde{\mathbf{y}}_t, \tilde{P}] - \mathbf{x}_0 \right)^T A^T A \mathbf{f}(\tilde{\mathbf{y}}_t, \tilde{P}) \right]. \quad (\text{A.6}) \end{aligned}$$

We will now work with the last term.

$$\mathbb{E}_{\mathbf{x}_0, \tilde{\mathbf{y}}_t, A, \tilde{P}} \left[\left(\mathbb{E}[\mathbf{x}_0 | \tilde{\mathbf{y}}_t, \tilde{P}] - \mathbf{x}_0 \right)^T A^T A \mathbf{f}(\tilde{\mathbf{y}}_t, \tilde{P}) \right] \quad (\text{A.7})$$

$$= \mathbb{E}_{\tilde{\mathbf{y}}_t, A, \tilde{P}} \left[\mathbb{E}_{\mathbf{x}_0 | \tilde{\mathbf{y}}_t, A, \tilde{P}} \left[\left(\mathbb{E}[\mathbf{x}_0 | \tilde{\mathbf{y}}_t, \tilde{P}] - \mathbf{x}_0 \right)^T A^T A \mathbf{f}(\tilde{\mathbf{y}}_t, \tilde{P}) \right] \right] \quad (\text{A.8})$$

$$= \mathbb{E}_{\tilde{\mathbf{y}}_t, A, \tilde{P}} \left[\left(\mathbb{E}[\mathbf{x}_0 | \tilde{\mathbf{y}}_t, \tilde{P}] - \mathbb{E}[\mathbf{x}_0 | \tilde{\mathbf{y}}_t, A, \tilde{P}] \right)^T A^T A \mathbf{f}(\tilde{\mathbf{y}}_t, \tilde{P}) \right] \quad (\text{A.9})$$

$$= 0, \quad (\text{A.10})$$

since $\mathbb{E}[\mathbf{x}_0|\tilde{\mathbf{y}}_t, \tilde{P}] = \mathbb{E}[\mathbf{x}_0|\tilde{\mathbf{y}}_t, A, \tilde{P}]$, i.e. the value of \mathbf{x}_0 does not depend on \tilde{A} given \tilde{P} and $\tilde{\mathbf{y}}_t$.

We will now work with the middle term. We have that:

$$\mathbb{E}_{\tilde{\mathbf{y}}_t, A, \tilde{P}} \left[\mathbf{f}(\tilde{\mathbf{y}}_t, \tilde{P})^T A^T A \mathbf{f}(\tilde{\mathbf{y}}_t, \tilde{P}) \right] \quad (\text{A.11})$$

$$= \mathbb{E}_{\tilde{\mathbf{y}}_t, \tilde{P}} \left[\mathbb{E}_{A|\tilde{\mathbf{y}}_t, \tilde{P}} \left[\mathbf{f}(\tilde{\mathbf{y}}_t, \tilde{P})^T A^T A \mathbf{f}(\tilde{\mathbf{y}}_t, \tilde{P}) \right] \right] \quad (\text{A.12})$$

$$= \mathbb{E}_{\tilde{\mathbf{y}}_t, \tilde{P}} \left[\mathbf{f}(\tilde{\mathbf{y}}_t, \tilde{P})^T \mathbb{E}[A^T A|\tilde{P}] \mathbf{f}(\tilde{\mathbf{y}}_t, \tilde{P}) \right]. \quad (\text{A.13})$$

From the last equation, it is evident that if $\mathbb{E}[A^T A|\tilde{P}]$ is full-rank, and hence the minimizer is $\mathbb{E}[\mathbf{x}_0|\tilde{\mathbf{y}}_t, \tilde{P}]$ as needed.

Since our A matrix is square, it suffices to show that $\mathbb{E}[A|\tilde{P}]$ is full-rank. By Corollary A.1. in Ambient Diffusion, we have that: $\mathbb{E}[P|\tilde{P}]$ is full-rank. We will now show that $\mathcal{F}^{-1}\mathbb{E}[P|\tilde{P}]\mathcal{F}$ is also full-rank. This can be easily proved with contradiction. Assume that $\mathcal{F}^{-1}\mathbb{E}[P|\tilde{P}]\mathcal{F}$ is not full-rank. Then, there exists a vector $\mathbf{w} \neq \mathbf{0}$ such that:

$$\mathcal{F}^{-1}\mathbb{E}[P|\tilde{P}]\mathcal{F}\mathbf{w} = 0 \iff \quad (\text{A.14})$$

$$\mathbb{E}[P|\tilde{P}] \underbrace{\mathcal{F}\mathbf{w}}_{\mathbf{z} \neq \mathbf{0}} = 0 \iff \quad (\text{A.15})$$

$$\mathbb{E}[P|\tilde{P}]\mathbf{z} = 0, \quad (\text{A.16})$$

which is a contradiction, since $\mathbf{z} \neq \mathbf{0}$ and $\mathbb{E}[P|\tilde{P}]$ is full-rank.

So far, we have established that $\mathcal{F}^{-1}\mathbb{E}[P|\tilde{P}]\mathcal{F}$ is full-rank. By linearity of expectation, we further have that:

$$\mathcal{F}^{-1}\mathbb{E}[P|\tilde{P}]\mathcal{F} = \mathbb{E}[\mathcal{F}^{-1}P\mathcal{F}|\tilde{P}], \quad (\text{A.17})$$

and hence, the latter is also full-rank. Finally, since $\sum_i S_i^H S_i = I$, for any full-rank matrix C , we have that $\sum_i S_i^H C S_i$ is also full-rank. This is true for any given set S_i and hence it is also true for the expectation over the sets $\{S_i\}$. Putting everything together, we have that:

$$\mathbb{E}_{\{S_i\}, P} \left[\sum_i S_i^H \mathcal{F}^{-1}\mathbb{E}[P|\tilde{P}]\mathcal{F} S_i \middle| \tilde{P} \right] = \mathbb{E}[A|\tilde{P}], \quad (\text{A.18})$$

is full-rank and the proof is complete. □

B Additional Performance Results

Here we include additional performance results.

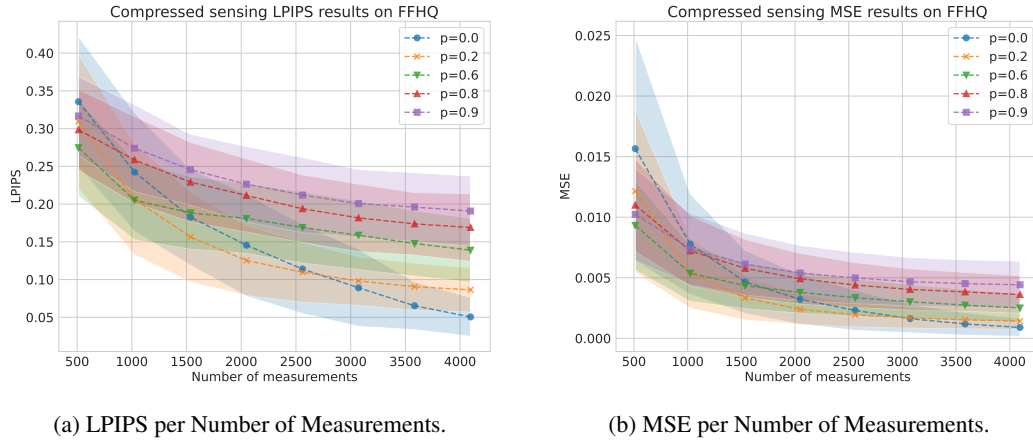


Figure 10: Compressed Sensing Results for FFHQ.

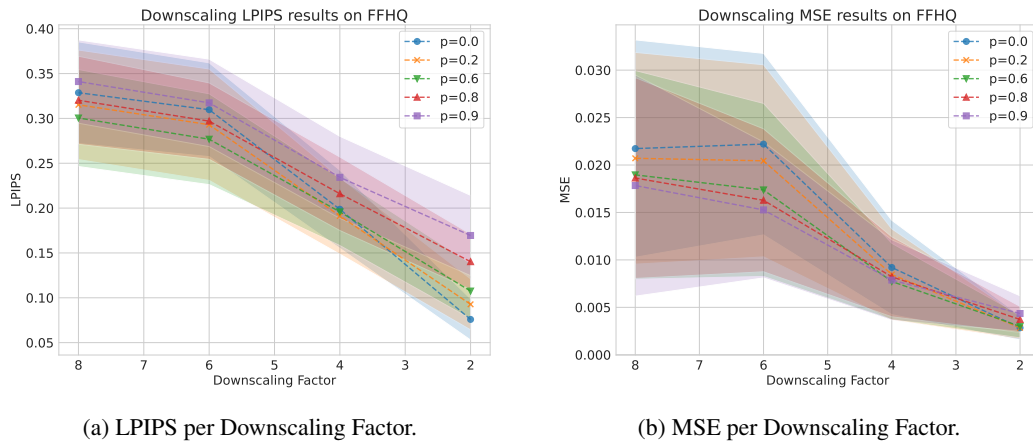


Figure 11: Downscaling Results for FFHQ.

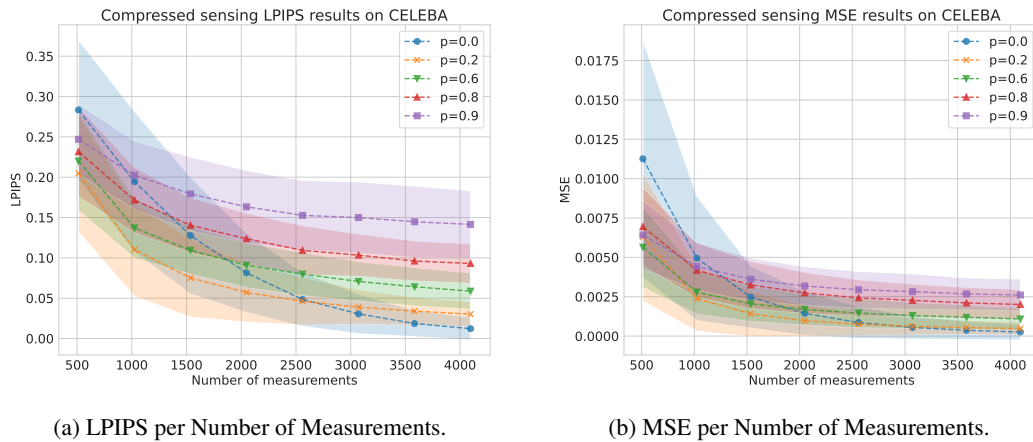
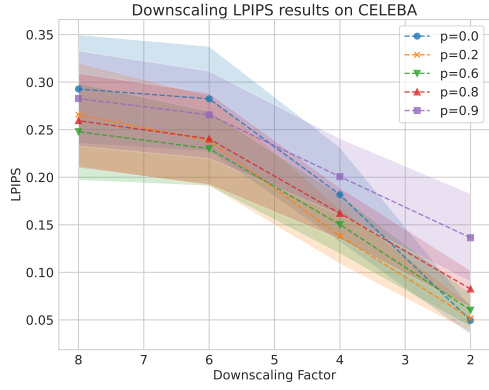
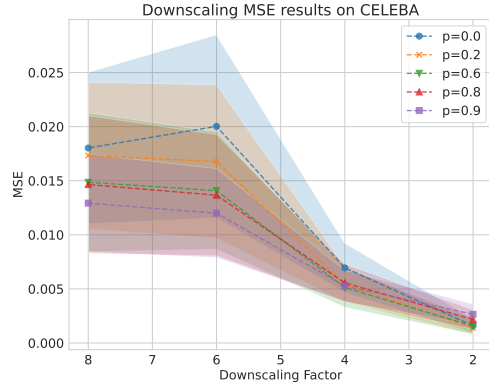


Figure 12: Compressed Sensing Results for Celeb-A.



(a) LPIPS per Downscaling Factor.

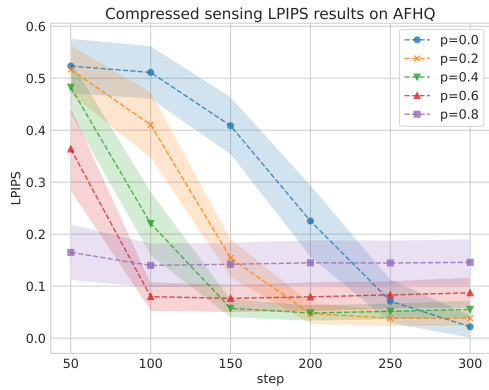


(b) MSE per Downscaling Factor.

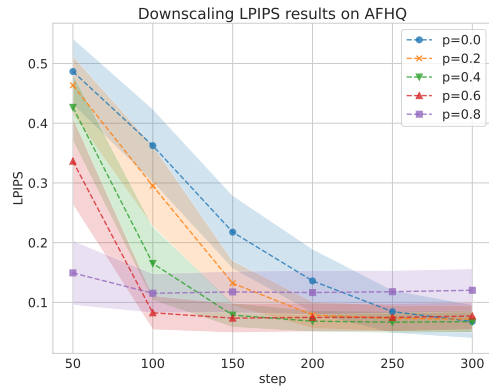
Figure 13: Downscaling Results for Celeb-A.

C Additional Speed Results

We further include additional speed results.

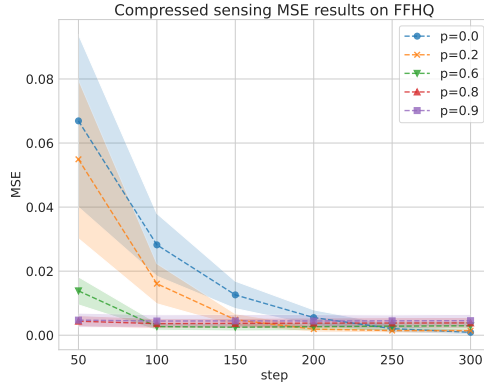


(a) Compressed Sensing with 4000 measurements per Number of Function Evaluations (NFEs).

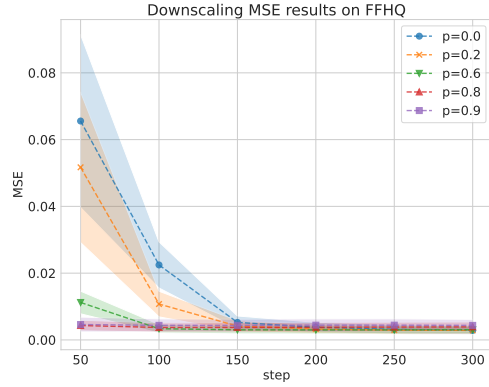


(b) $2\times$ Super-Resolution per Number of Function Evaluations (NFEs).

Figure 14: Speed LPIPS performance plots for AFHQ.

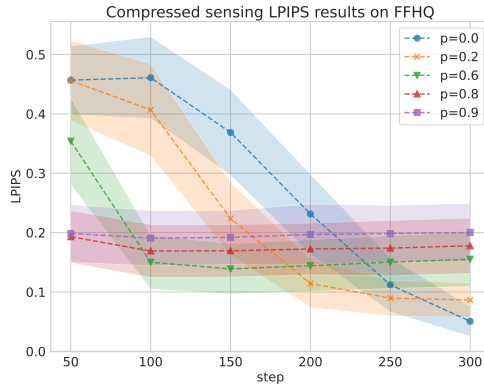


(a) Compressed Sensing with 4000 measurements per Number of Function Evaluations (NFEs).

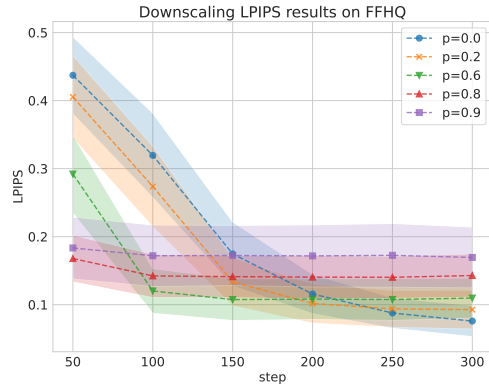


(b) $2\times$ Super-Resolution per Number of Function Evaluations (NFEs).

Figure 15: Speed MSE performance plots for FFHQ.

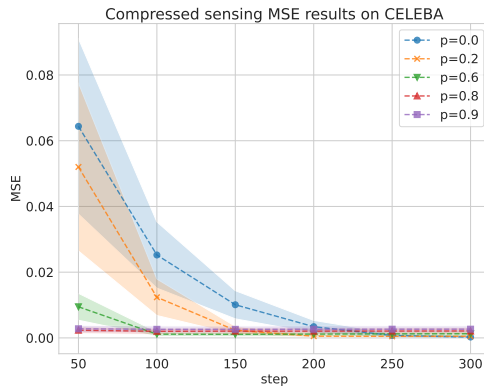


(a) Compressed Sensing with 4000 measurements per Number of Function Evaluations (NFEs).

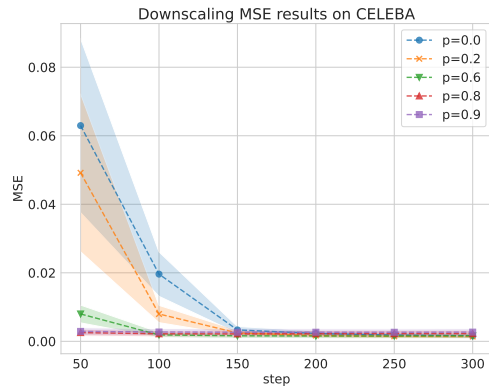


(b) $2\times$ Super-Resolution per Number of Function Evaluations (NFEs).

Figure 16: Speed LPIPS performance plots for FFHQ.

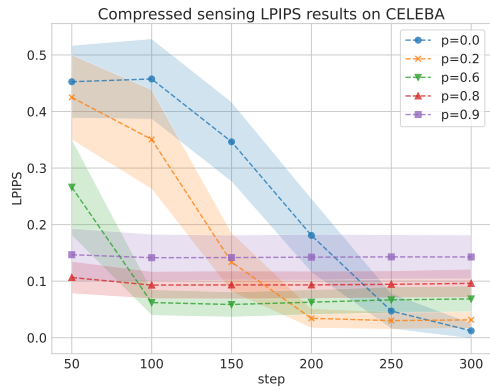


(a) Compressed Sensing with 4000 measurements per Number of Function Evaluations (NFEs).

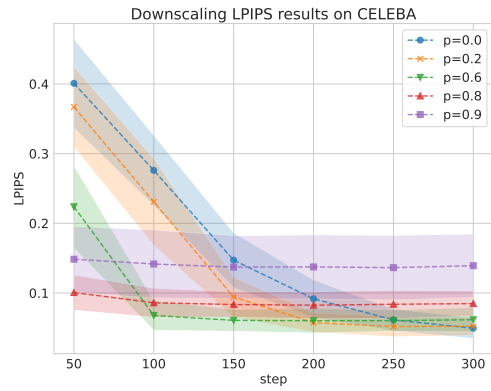


(b) $2\times$ Super-Resolution per Number of Function Evaluations (NFEs).

Figure 17: Speed MSE performance plots for Celeb-A.



(a) Compressed Sensing with 4000 measurements per Number of Function Evaluations (NFEs).



(b) $2\times$ Super-Resolution per Number of Function Evaluations (NFEs).

Figure 18: Speed LPIPS performance plots for Celeb-A.

D Additional MRI Results

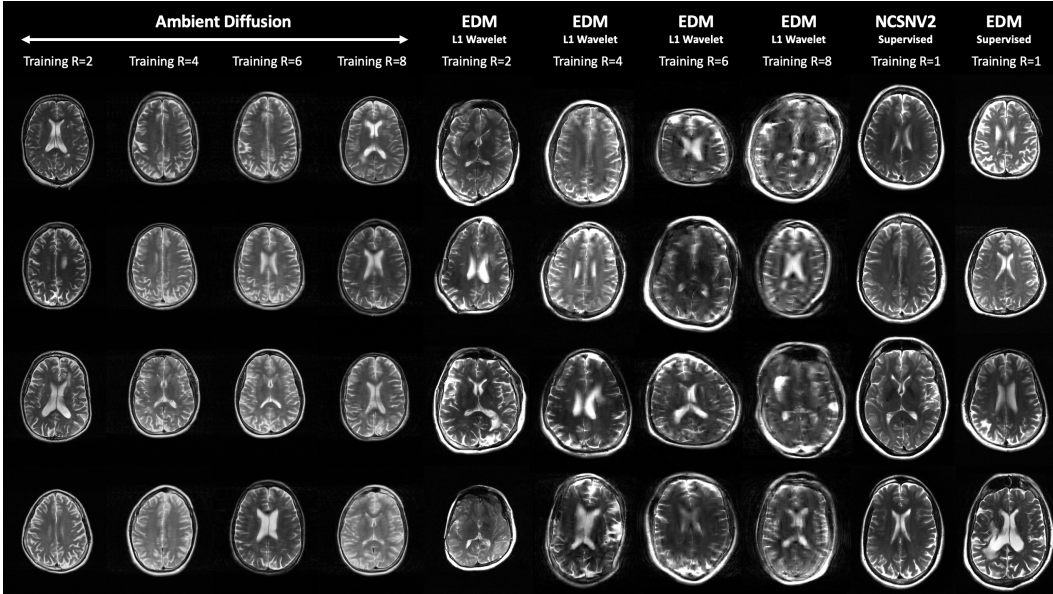


Figure 19: Prior samples from Ambient Diffusion trained with under sampled data at $R = 2, 4, 6, 8$ (columns 1 – 4), EDM trained with L1-wavelet reconstructions of subsampled data at $R = 2, 4, 6, 8$ (columns 5 – 8), NCSNV2 trained with fully sampled data (column 9) and EDM trained with fully sampled data (column 10).

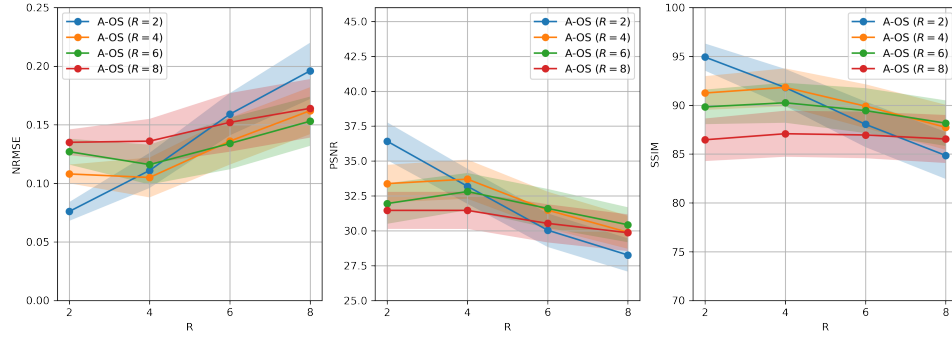


Figure 20: Ambient diffusion one step performance metrics at $R = 2, 4, 6, 8$ for models trained at $R = 2, 4, 6, 8$.

E Training Hyperparameters for MRI models

The EDM model trained on the fully-sampled ($R = 1$) dataset, as well as the four EDM models trained on L1-Wavelet reconstructions at each acceleration factor $R \in \{2, 4, 6, 8\}$ were all trained with 65 million parameters. The Ambient Diffusion models on the other hand were trained with 36 million parameters, for faster training. All the Ambient Diffusion models were trained for 250 epochs. For the Ambient Diffusion training experiments, the further corrupted sampling masks are given as an input to the model by concatenating with the measurements along the channel dimension, as in the original Ambient Diffusion [17] paper.

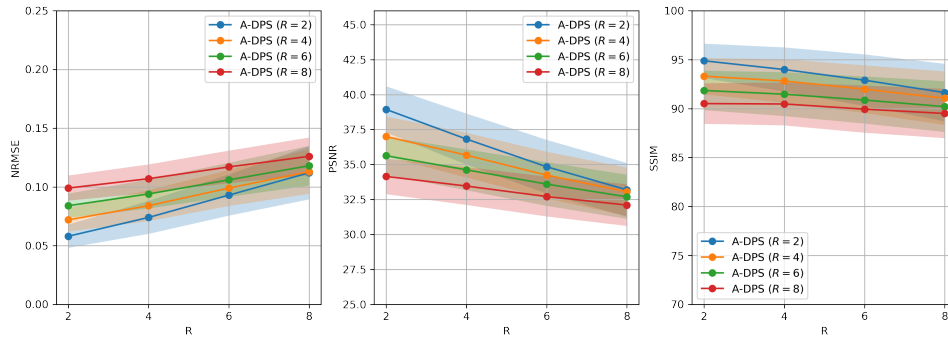


Figure 21: Ambient diffusion posterior sampling multi-step performance metrics at $R = 2, 4, 6, 8$ for models trained at $R = 2, 4, 6, 8$.

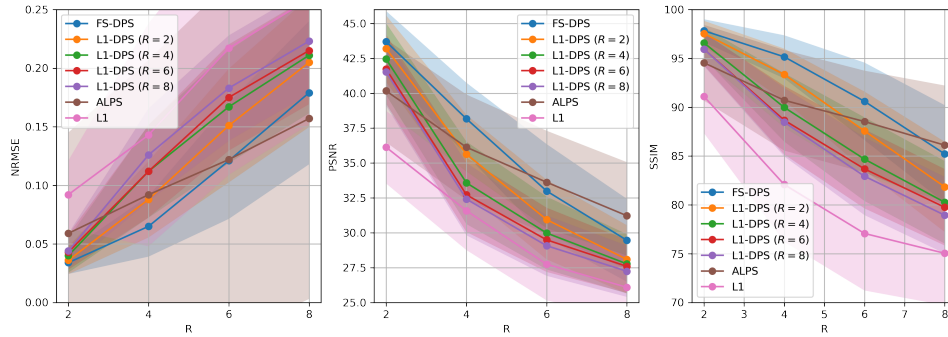


Figure 22: Performance metrics at $R = 2, 4, 6, 8$ for L1-wavelet compressed sensing, diffusion/score-based models trained with fully sampled data (FS-DPS, ALPS), diffusion models trained with L1 reconstructions of subsampled data (L1-DPS)

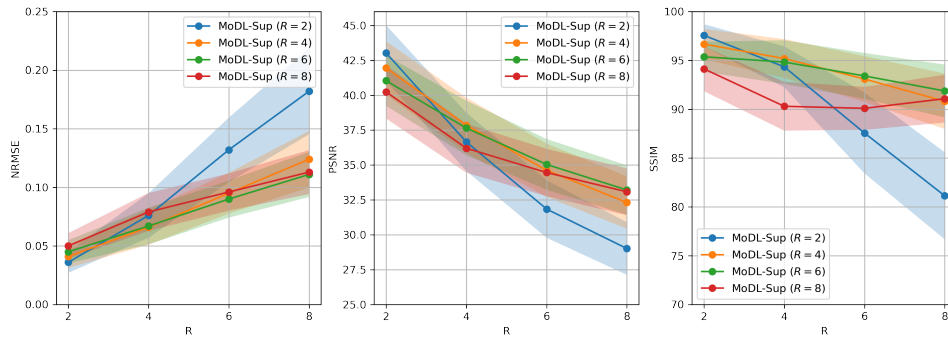


Figure 23: Fully supervised MoDL performance metrics at $R = 2, 4, 6, 8$ for models trained at $R = 2, 4, 6, 8$.

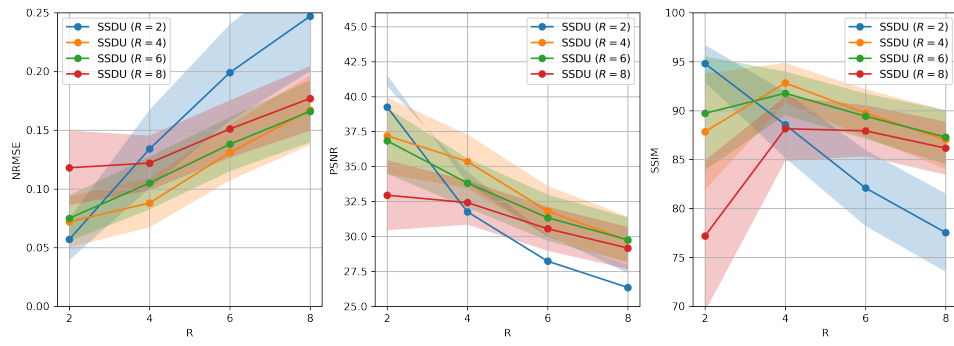


Figure 24: SSDU MoDL performance metrics at $R = 2, 4, 6, 8$ for models trained at $R = 2, 4, 6, 8$.